ACS APPLIED MATERIALS & INTERFACES

Research Article

www.acsami.org

Detecting Liquefied Petroleum Gas (LPG) at Room Temperature Using $ZnSnO_3$/ZnO Nanowire Piezo-Nanogenerator as Self-Powered Gas Sensor

Yongming Fu,[†] Yuxin Nie,[†] Yayu Zhao,[†] Penglei Wang,[†] Lili Xing,[†] Yan Zhang,*[,‡,§] and Xinyu Xue*[,†]

[†]College of Sciences, Northeastern University, Shenyang 110004, China

[‡]Institute of Theoretical Physics, Lanzhou University, Lanzhou 730000, China

[§]Beijing Institute of Nanoenergy and Nanosystems, Chinese Academy of Sciences, Beijing 100000, China

ABSTRACT: High sensitivity, selectivity, and reliability have been achieved from $ZnSnO_3$/ZnO nanowire (NW) piezo-nanogenerator (NG) as self-powered gas sensor (SPGS) for detecting liquefied petroleum gas (LPG) at room temperature (RT). After being exposed to 8000 ppm LPG, the output piezo-voltage of $ZnSnO_3$/ZnO NW SPGS under compressive deformation is 0.089 V, much smaller than that in air ambience (0.533 V). The sensitivity of the SPGS against 8000 ppm LPG is up to 83.23, and the low limit of detection is 600 ppm. The SPGS has lower sensitivity against H_2S, H_2, ethanol, methanol and saturated water vapor than LPG, indicating good selectivity for detecting LPG. After two months, the decline of the sensing performance is less than 6%. Such piezo-LPG sensing at RT can be ascribed to the new piezo-surface coupling effect of $ZnSnO_3$/ZnO nanocomposites. The practical application of the device driven by human motion has also been simply demonstrated. This work provides a novel approach to fabricate RT-LPG sensors and promotes the development of self-powered sensing system.

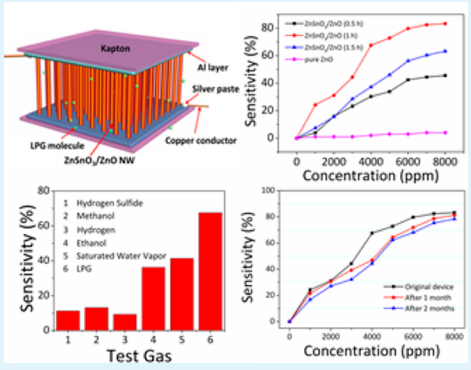

KEYWORDS: *nanogenerator, $ZnSnO_3$/ZnO nanowire, self-powered, liquefied petroleum gas, gas sensing*

INTRODUCTION

Recently, the energy crisis and air pollution are among the most serious problems facing the world.[1−4] Much research effort has been made on developing new technologies in the fields of green energy harvesting and gas sensing.[5−8] Most recently, considering that ZnO nanowires (NWs) have both the gas sensing and piezoelectric properties, unpackaged ZnO NW piezo-nanogenerator (NG) used as a new self-powered gas sensor (SPGS) has been demonstrated.[9] The piezoelectric output of ZnO NW SPGS generated by the tiny mechanical vibration in the environment can both drive the device and act as a room-temperature (RT) gas sensing signal. In different gas ambience (H_2S, O_2, dry/humid air) at RT, the output piezo-voltage of ZnO NW SGPS is different, showing a good potential for realizing gas sensing at RT.[9]

As a common gaseous fuel, liquefied petroleum gas (LPG) has important applications in kitchens and industrial factories.[10−13] However, detecting flammable LPG at RT remains a challenge.[14−16] It has been demonstrated that some perovskite-type ternary compounds (ABO_3), such as $ZnSnO_3$, $CdSnO_3$, and $ZnTiO_3$, have effective sensing characteristics against organic gas at RT.[17−22] Thus, it is highly expected that introducing $ZnSnO_3$/ZnO heterostructures into the SGPS can obtain piezo-LPG sensing at RT through the synergistic effect between the two components.

In this work, piezo-LPG sensing with high sensitivity, selectivity, and reliability at RT has been obtained from $ZnSnO_3$/ZnO NW SPGS. The RT-LPG sensing can be ascribed to the new piezo-surface coupling effect of $ZnSnO_3$/ZnO nanocomposites. The present results can provoke a right direction for realizing LPG sensing at RT.

EXPERIMENTAL SECTION

As the first step, ZnO NWs were prepared via a seed-assisted hydrothermal route. A piece of precleaned Ti foil was used as both the substrate and current collector (Figure 1a) and was deposited with a ZnO seed layer by a previous method (Figure 1b).[9] Then, 0.744 g of $Zn(NO_3)_2{\cdot}6H_2O$ and 0.350 g of hexamethylene tetramine (HMTA) were added into 200 mL of distilled water, and the Ti substrate was immersed into the solution. The reaction flask was sealed and kept at 93 °C for 2 h. The Ti substrate with ZnO NW grown on was collected, rinsed with ethanol/water, and dried at 60 °C, as shown in Figure 1c.

As the second step, $ZnSnO_3$/ZnO NWs were synthesized via a corrosion process of ZnO NWs (Figure 1d). $Na_2SnO_3{\cdot}4H_2O$ (0.16 g) and H_2NCONH_2 (1.45 g) were added into 50 mL of ethanol/water (60 vol % of ethanol) solvents and stirred for forming a homogeneous solution. The Ti substrate with ZnO NWs grown on was vertically positioned in a Teflon-lined stainless steel autoclave (volume = 60 mL), and the above solution was transferred into the autoclave. The

Received: March 4, 2015
Accepted: April 27, 2015
Published: April 27, 2015

DOI: 10.1021/acsami.5b01822
ACS Appl. Mater. Interfaces 2015, 7, 10482−10490

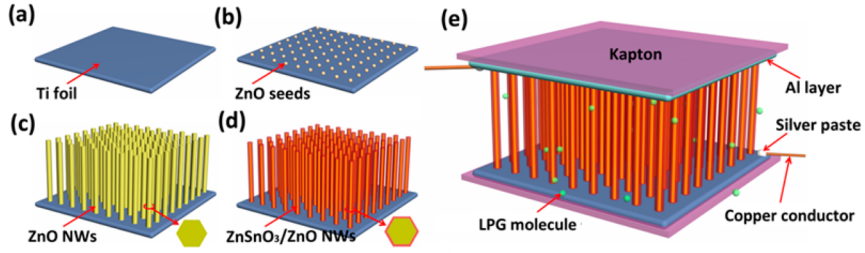

Figure 1. Fabrication process of $ZnSnO_3$/ZnO NW SPGS: (a and b) ZnO seeds are deposited on the precleaned Ti foil; (c) ZnO NWs are vertically aligned on the substrate via a hydrothermal route; and (d) $ZnSnO_3$/ZnO NWs are obtained through the corrosion process. (e) The device structure.

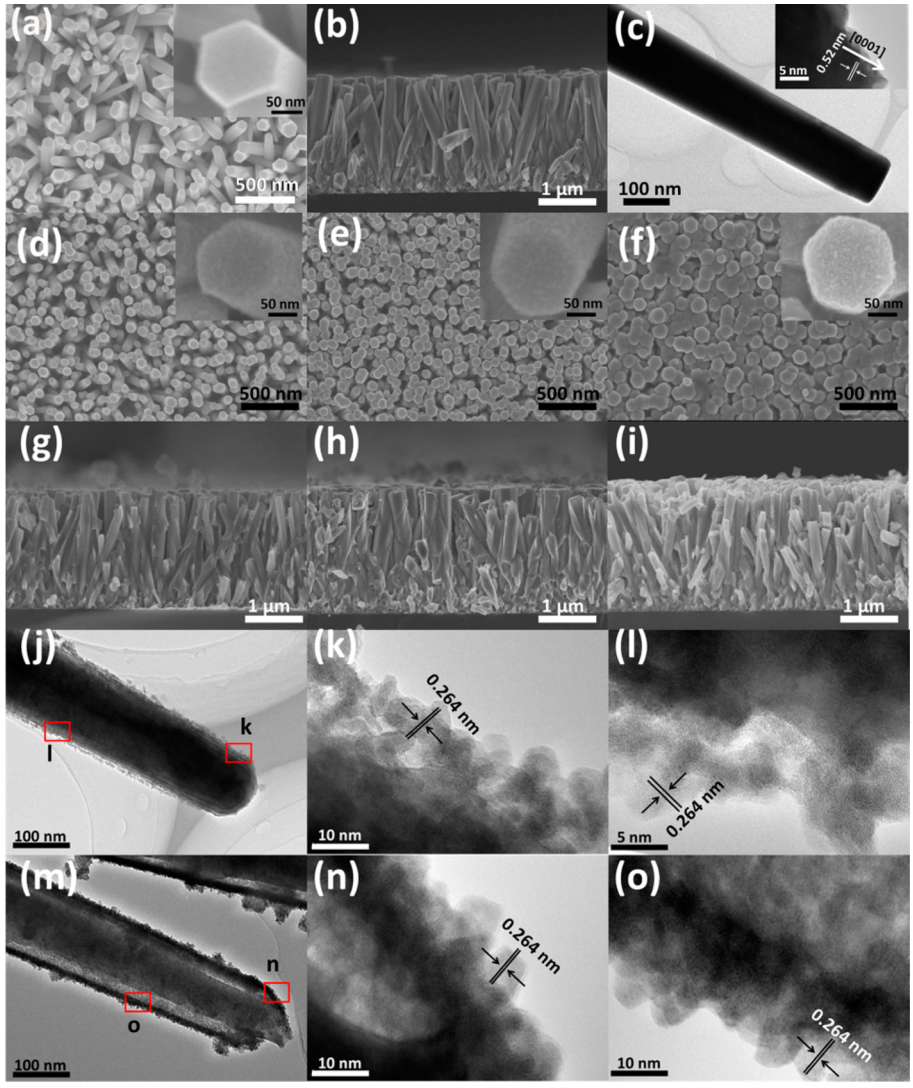

Figure 2. (a–c) SEM and TEM images of pure ZnO NWs; (c, inset) HRTEM image of pure ZnO NW. Top-view SEM images of (d) $ZnSnO_3$/ZnO (0.5 h), (e) $ZnSnO_3$/ZnO (1 h), and (f) $ZnSnO_3$/ZnO (1.5 h) NWs; (insets) enlarged views of the tip regions. Side-view SEM images of (g) $ZnSnO_3$/ZnO (0.5 h), (h) $ZnSnO_3$/ZnO (1 h), and (i) $ZnSnO_3$/ZnO (1.5 h) NWs. (j–l) TEM and HRTEM images of $ZnSnO_3$/ZnO (0.5 h) NW. (m–o) TEM and HRTEM images of $ZnSnO_3$/ZnO (1 h) NW.

autoclave was sealed and maintained at 170 °C for 1 h. After being cooled down to RT, the Ti foil with $ZnSnO_3$/ZnO NWs grown on was collected, washed with ethanol/water, and finally dried at 60 °C. The amount of $ZnSnO_3$ contents were controlled by changing the reaction time (0, 0.5, 1, and 1.5 h).

Figure 1e shows that the SPGS is made up of the following major parts: $ZnSnO_3$/ZnO NWs on Ti substrate, a piece of Al foil and two polyimide (PI/Kapton) films. The Ti foil is used as both the substrate for supporting the NWs and the current collector for the electric measurement. The Al foil (thickness = 50 μm) on the tips of the NWs acts as the opposite current collector. The two PI films as the frame are used to support the whole device. The Ti and Al foils are the two electrodes for the electric measurement through copper leads and silver glue. The SPGS is fixed in a gas-flow chamber (volume = 10 L), and applied with a constant compressive force (1 Hz, 30 N). The output piezo-voltage of the SPGS in different concentrations of LPG is measured with the external circuit. The LPG concentration in the chamber is calibrated using volume ratio, and a certain volume of LPG

DOI: 10.1021/acsami.5b01822
ACS Appl. Mater. Interfaces 2015, 7, 10482–10490

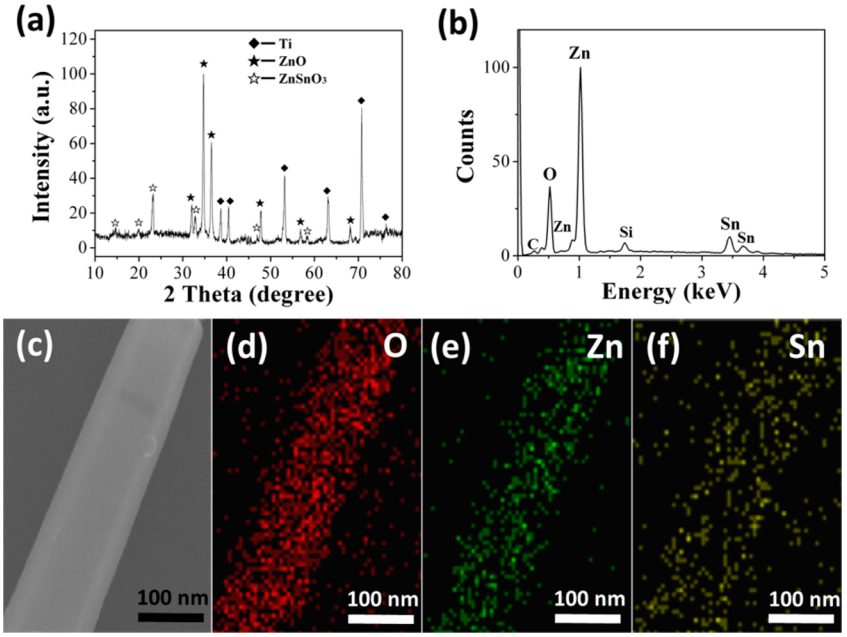

Figure 3. (a) XRD pattern and (b) EDS spectrum of $ZnSnO_3$/ZnO (1 h) NWs. (c–f) Elemental mapping crossing one single $ZnSnO_3$/ZnO (1 h) NW.

is injected into the chamber by an injector. For example, 1000 ppm LPG is obtained by injecting 10 mL of pure LPG into the chamber. Under the compressive deformation, a piezoelectric potential can be generated along the length direction of ZnO NWs as the core in the core–shell structures (output piezo-voltage), and $ZnSnO_3$ nanoparticles as the shell have LPG sensing characteristics at RT and can vary the piezo-voltage in different concentration of LPG through the gas-dependent piezo-screening effect.[9,20,23−25]

RESULTS AND DISCUSSION

Figure 2 shows the morphology and microstructure of pure ZnO and $ZnSnO_3$/ZnO NWs. Figure 2a shows a typical

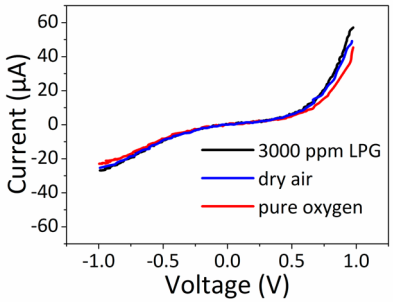

Figure 4. *I*–*V* behaviors of $ZnSnO_3$/ZnO (1 h) NWs in different ambience at RT without applied deformation.

scanning electron microscopy (SEM; JEOL JSM-6700F) image of pure ZnO NWs on the top view, indicating that almost all of the NWs are vertically grown on Ti foil. The enlarged view of the tip region is inserted on the right top corner, indicating a hexagonal shape (wurtzite ZnO) with smooth surface. Figure 2b shows an SEM image of pure ZnO NWs on the side view, further demonstrating that the NWs are grown along a uniform direction. Figure 2c shows a transmission electron microscopy (TEM; JEOL JEM-2010) image of pure ZnO NW, revealing that the diameter is about 120 nm. The inset of Figure 2c is a

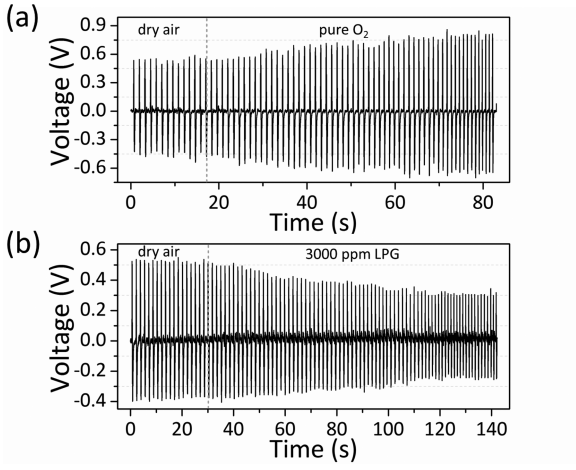

Figure 5. Continuous response of the piezoelectric sensor ($ZnSnO_3$/ZnO (1 h) NWs) under a constant compressive force (1 Hz, 30 N) upon exposure to (a) pure oxygen and (b) 3000 ppm LPG.

high-resolution TEM (HRTEM) image of pure ZnO NW, clearly indicating the single-crystalline nature of the NW grown along the *c* axis. Figure 2d–f shows SEM images of $ZnSnO_3$/ZnO (0.5 h), $ZnSnO_3$/ZnO (1 h), and $ZnSnO_3$/ZnO (1.5 h) NWs on the top view, and the insets are the enlarged views of the tip regions. It can be seen that ZnO NWs are coated with a layer of $ZnSnO_3$ nanoparticles and the diameter of the NWs increases with increasing reaction time. Figure 2g–i shows SEM images of $ZnSnO_3$/ZnO (0.5 h), $ZnSnO_3$/ZnO (1 h), and $ZnSnO_3$/ZnO (1.5 h) NWs on the side view. The average length of the NWs slightly increases with increasing reaction time. Figure 2j is a TEM image of $ZnSnO_3$/ZnO (0.5 h) NW, showing that $ZnSnO_3$ nanoparticles uniformly cover on the whole surface of ZnO NW. The diameter of $ZnSnO_3$/ZnO (0.5 h) NWs is about 130 nm. Figure 2k,l shows HRTEM images of $ZnSnO_3$/ZnO (0.5 h) NW. The lattice fringe spacing of the nanoparticles on the surface of the NW is 0.264 nm,

DOI: 10.1021/acsami.5b01822
ACS Appl. Mater. Interfaces 2015, 7, 10482−10490

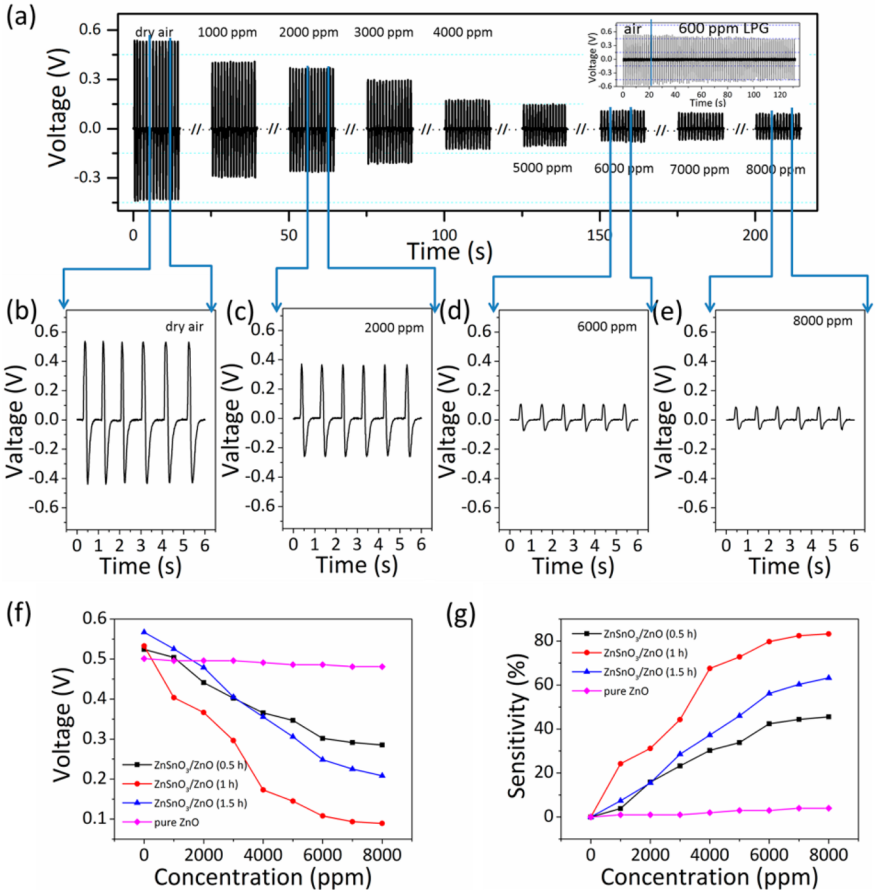

Figure 6. (a) Piezo-voltage of $ZnSnO_3$/ZnO (1 h) NW SPGS in dry air and different concentration of LPG under the same applied compressive force (1 Hz, 30 N); (inset) low limit of detection. Details of the piezo-voltage in (b) dry air and in (c) 2000, (d) 6000, and (e) 8000 ppm LPG. (f) Relationship between the piezo-voltage and the concentration of LPG. (g) Relationship between the sensitivity and the concentration of LPG.

Table 1. Comparison of LPG Sensing Performance between Our Results and Previous Works

materials	type	C (ppm)	T (°C)	S (%)	ref
Pd-ZnO films	resistive	4000	275	57	14
NiO films	resistive	3000	425	36.5	15
CdO films	resistive	600	425	15	16
$ZnSnO_3$ films	resistive	10000	25	38	20
Zn_2SnO_4/ZnO nanorods	resistive	3000	250	63	24
Al-ZnO films	resistive	5000	325	77	28
$BaTiO_3$ films	resistive	5000	300	45	29
ZnO films	resistive	5200	400	49	30
pure ZnO NWs	piezoelectric	4000	RT	2.99	this work
$ZnSnO_3$/ZnO NWs	piezoelectric	4000	RT	67.52	this work

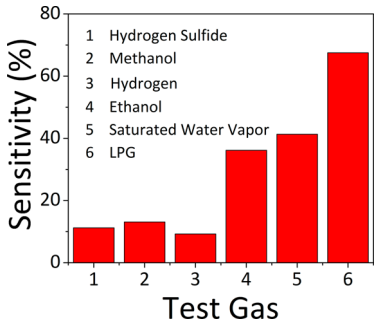

Figure 7. Sensitivity of $ZnSnO_3$/ZnO (1 h) NW SPGS upon exposure to 4000 ppm of H_2S, H_2, ethanol, methanol, LPG and saturated water vapor.

corresponding to $ZnSnO_3$ (110) plane. Figure 2m shows a TEM image of $ZnSnO_3$/ZnO (1 h) NW, indicating that the nanoparticle layer of $ZnSnO_3$/ZnO (1 h) NW is thicker than that of $ZnSnO_3$/ZnO (0.5 h) NW. The diameter of $ZnSnO_3$/ZnO (1 h) NWs is about 150 nm. Figure 2n,o shows HRTEM images of $ZnSnO_3$/ZnO (1 h) NW. With longer reaction time, more $ZnSnO_3$ nanoparticles cover the surface of ZnO NWs. On the basis of these features, we can determine that the layer of $ZnSnO_3$ nanoparticles is produced through the corrosion process on the surface of ZnO. First, the reaction solution corrodes ZnO NWs from the surface and produces Zn^{2+} ions. Then, SnO_3^{2-} ions react with these Zn^{2+} ions and produce $ZnSnO_3$ nanoparticles that evenly cover on the surface of ZnO.[26] In this process, the space between $ZnSnO_3$ nanoparticles contributes to the increased NW diameter.

Figure 3 shows the crystal structure and component of $ZnSnO_3$/ZnO NWs. Figure 3a shows an X-ray powder diffraction (XRD; D/max 2550 V, Cu Kα radiation, λ = 1.5416 Å) pattern of $ZnSnO_3$/ZnO (1 h) NWs. The diffraction peaks indexed to Ti (JCPDS file no. 44-1294) arise from the Ti foil substrate, and the other diffraction peaks can be indexed to perovskite-type $ZnSnO_3$ (JCPDS file no. 28-1486) and ZnO (JCPDS file no. 36-1451), respectively. Figure 3b shows energy dispersive spectrometer (EDS) spectrum of $ZnSnO_3$/ZnO (1

DOI: 10.1021/acsami.5b01822
ACS Appl. Mater. Interfaces 2015, 7, 10482−10490

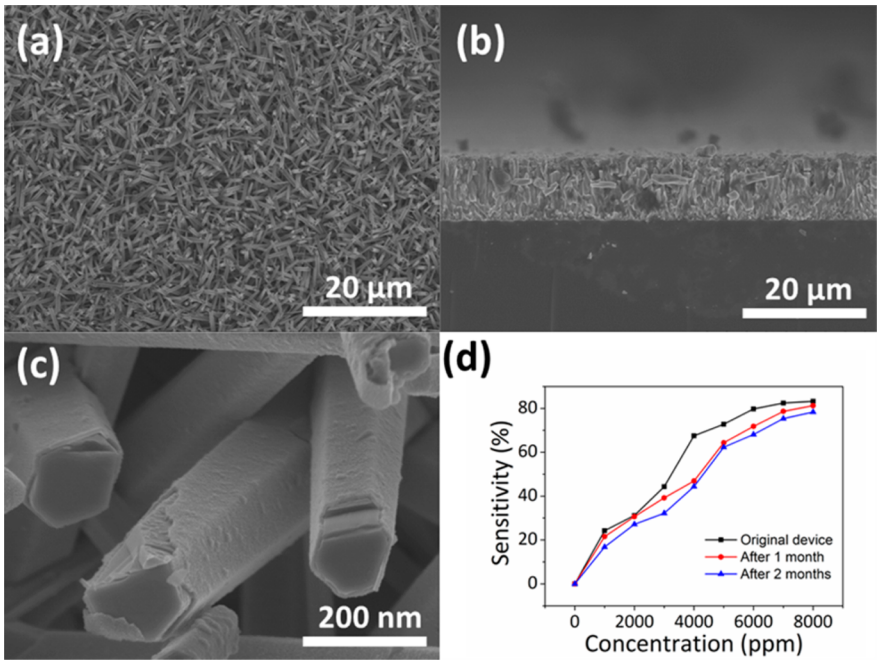

Figure 8. (a and b) SEM images of $ZnSnO_3$/ZnO (1 h) NWs after 50 000 time deformations on the top and side views, respectively. (c) Tips of the NWs. (d) Sensitivity decline within two months.

h) NW. For the investigation of the element component of individual NWs, the NWs are exfoliated from Ti substrate, dispersed in ethanol, and transferred to Si wafer for separate measuring. Five elements (Sn, Zn, O, Si, and C) can be observed from the spectrum (the peaks of Si and C arise from Si wafer substrate and carbon conductive adhesive tape, respectively). EDS measurements have been conducted on several other NWs, and Sn, Zn, and O elements can be detected in each NW. Figure 3c–f shows the elemental mapping crossing one single $ZnSnO_3$/ZnO (1 h) NW. Sn element can be detected along the surface of the sample with uniform distribution, further confirming that $ZnSnO_3$ layer exists as the shell of the NWs. These results indicate that ZnO NWs are uniformly coated with $ZnSnO_3$ nanoparticles with good crystalline quality.

Figure 4 exhibits the $I-V$ behavior of $ZnSnO_3$/ZnO (1 h) NWs in different gas ambience at RT (no force is applied on the device). The nonlinear $I-V$ characteristics can be ascribed to the asymmetric Schottky barriers (NW/Al and NW/Ti).[27] The resistive response of $ZnSnO_3$/ZnO (1 h) NWs against LPG is not high. After sufficient time for full adsorption, the current of the device (the bias voltage is 1 V) upon exposure to 3000 ppm LPG increases from 49.2 (in dry air) to 57.1 μA. In pure oxygen, the current is 45.4 μA. The corresponding resistive-sensitivity (S_R) of the device against pure oxygen and 3000 ppm LPG is merely 7.72 and 16.06, respectively. The resistive sensitivity can be defined as

$$S_R\ (\%) = \frac{|R_a - R_g|}{R_a} \times 100 \qquad (1)$$

in which R_g and R_a represent the resistance in test gas and dry air, respectively. Although the surface adsorption of LPG molecules or oxygen ions can influence the carrier density of $ZnSnO_3$ nanoparticles and vary the effective barrier at $ZnSnO_3$/ZnO interface (the work function of n-type $ZnSnO_3$ and ZnO is 5.3 and 4.5 eV, respectively.[20]), such modification of the conductance is very limited at RT and can hardly affect the $I-V$ behavior of the device. The low sensitivity restrains their applications as traditional resistive-type LPG sensors.

In contrast to the $I-V$ behavior, the gas atmosphere can greatly influence the piezoelectric output of $ZnSnO_3$/ZnO NW SPGS, as shown in Figure 5. Figure 5a,b show the continuous response of $ZnSnO_3$/ZnO (1 h) NW SPGS at RT against pure oxygen and 3000 ppm LPG, respectively. In dry air ambience, the output piezo-voltage of the SPGS under the compressive deformation is 0.533 V. After changing the ambience to pure oxygen, the piezo-voltage of the SPGS under the same deformation condition increases to 0.793 V. Upon exposure to 3000 ppm LPG, the piezo-voltage of the SPGS decreases to about 0.297 V. The response time of the SPGS can be simply defined as the time for reaching stable piezo-voltage again after changing the surrounding gas ambience. The response time against pure oxygen and LPG at RT is about 72 and 88 s, respectively.

The piezoelectric output of the SPGS not only can drive the device but also can be regarded as the sensing signal for detecting different concentration of LPG, as shown in Figure 6. The measurements are conducted at RT, and $ZnSnO_3$/ZnO NW SPGSs are applied with same applied force (1 Hz, 30 N). From Figure 6a, it can be observed that the piezo-voltage of $ZnSnO_3$/ZnO (1 h) NWs is dependent on the LPG concentration in the environment. The piezo-voltage of the device (0.533 V in dry air) at RT against 1000, 2000, 3000, 4000, 5000, 6000, 7000, and 8000 ppm LPG is 0.404, 0.367, 0.297, 0.173, 0.145, 0.108, 0.094, and 0.089 V, respectively. The low limit of detection of the device against LPG is about 600 ppm (~0.450 V), as shown in the inset of Figure 6a. Figure 6b–e shows enlarged views of the piezo-voltage of the SPGS in dry air, 2000, 6000, and 8000 ppm LPG, respectively. The LPG-concentration-dependent piezo-voltage of the SPGSs with different $ZnSnO_3$ contents is shown in Figure 6f. The piezo-LPG-sensing behavior is related to the $ZnSnO_3$ content. The

DOI: 10.1021/acsami.5b01822
ACS Appl. Mater. Interfaces 2015, 7, 10482–10490

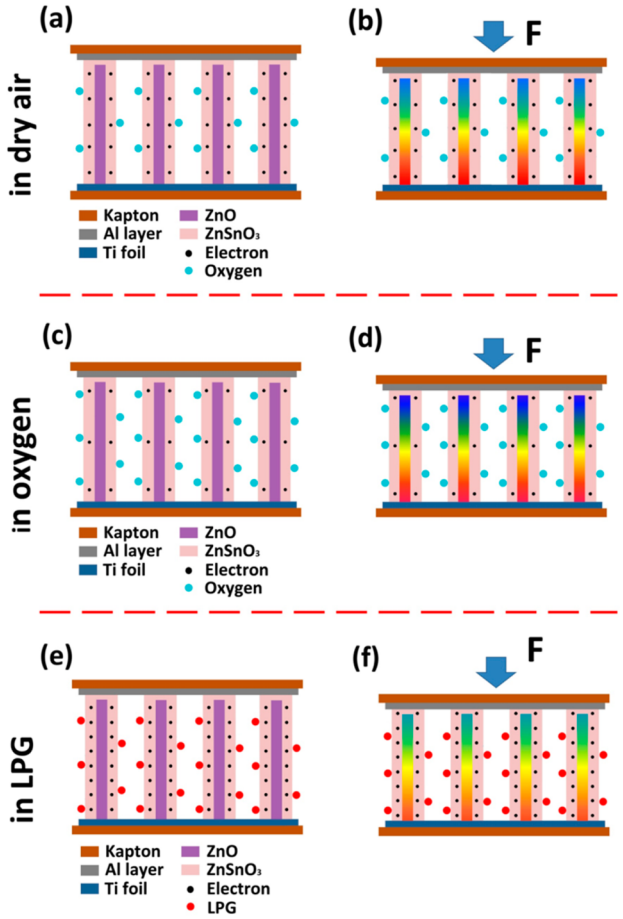

Figure 9. Working mechanism of $ZnSnO_3$/ZnO NW SPGS. (a) Without any applied deformation in dry air. (b) Applying a compressive force on the device in dry air. (c) Without any applied deformation in pure oxygen. (d) Applying a compressive force on the device in pure oxygen. (e) Without any applied deformation in LPG. (f) Applying a compressive force on the device in LPG.

piezo-sensitivity (S) of the SPGS for detecting LPG under the same applied force can be simply defined as

$$S\ (\%) = \frac{|V_a - V_g|}{V_a} \times 100 \tag{2}$$

in which V_g and V_a represent the piezo-voltage in LPG and dry air, respectively. The LPG-concentration-dependent sensitivity of the SPGSs with different $ZnSnO_3$ contents is shown in Figure 6g. The sensitivity of $ZnSnO_3$/ZnO (1 h) NWs is the highest among the samples (0, 0.5, 1, and 1.5 h), indicating that the optimum reaction time for coating $ZnSnO_3$ nanoparticles is 1 h. The sensitivity of $ZnSnO_3$/ZnO (1 h) NWs is up to 24.22, 31.16, 44.31, 67.52, 72.78, 79.72, 82.41, and 83.23 against 1000−8000 ppm LPG, respectively. With the concentration of LPG higher than 7000 ppm, the sensitivity reaches saturation. The sensitivity of piezo-LPG sensing is higher than that of the I−V behavior in Figure 4. The comparison of LPG sensing behavior between our results and other previous works is shown in Table 1.[14−16,20,24,28−30] It can be concluded that the operation temperature of $ZnSnO_3$/ZnO NW SPGS can be lowered to RT, and its sensitivity is relatively high. Such RT-LPG sensing implies that $ZnSnO_3$/ZnO NW SPGS has potential applications for detecting LPG at the industrial level.

Selectivity is one of the most important and challenging aspects of gas sensors. To check the selectivity of $ZnSnO_3$/ZnO NW SPGS (distinguishing LPG among different gases), the sensitivities of $ZnSnO_3$/ZnO (1 h) NWs upon exposure to 4000 ppm of H_2S, H_2, ethanol, methanol, LPG and saturated water vapor are measured, respectively (Figure 7). And the sensitivity is 11.21, 13.11, 36.18, 9.25, 67.52 and 41.30, respectively, indicating a relatively high selectivity for LPG detection.

Reliability is another significant aspect of gas sensing system, especially for its practical applications. Figure 8 exhibits the reliability of $ZnSnO_3$/ZnO (1 h) NW SPGS. Figure 8a,b shows SEM images of the NWs after ~50 000 time deformations on the top and side views. Figure 8c shows the enlarged view of the tips of the NWs, and the fracture of the NWs does not take place in large area. As shown in Figure 8d, after 1 and 2 months, the decline of the sensing performance is about 2.37 and 5.88%, respectively, indicating a relatively high reliability for LPG detection.

The RT-LPG sensing of $ZnSnO_3$/ZnO NW SPGS can be ascribed to the new piezo-surface coupling effect of the nanocomposites. The piezoelectric effect is understood as when piezoelectric material is applied under mechanical stress and deformed, internal polarization takes place, and positive charge appears on one surface while negative charge appears on the opposite surface.[31] The surface effect is a mechanism that the specific surface area and the number of surface atoms significantly increase with decreasing diameter of material, leading to the high chemical/physical activity (such as highly sensitive gas sensing).[32] The common point of these two effects is "surface", and thus, they can probably be coupled together to form a new coupling effect (atmosphere can vary the piezo-screening effect and thus change the piezoelectric output).[9,27,33,34]

According to our previous theoretical works, while neglecting the carrier effect, the open-circuit piezo-voltage (V_{oc}) of the NG can be given by[35,36]

$$V_{oc} = \frac{e_{33} s_{33} d}{\varepsilon_s} \tag{3}$$

in which s_{33} is the strain of the material, d is the distance between the two current collectors, ε_s is the permittivity of the material, and e_{33} is piezoelectric constant. Considering the carriers in piezoelectric semiconductor, the piezo-potential will decrease as the piezoelectric charges can be screened by the surface carriers. In addition, the output voltage is nonlinear function of carrier density. For simplicity, the inverse proportion relationship can be considered as good approximation to previous theoretical results.[37] Therefore, the output piezo-voltage (V_{out}) of the SPGS can be given by

$$V_{out} = \frac{\gamma e_{33} s_{33} d}{\varepsilon_s N_D} \tag{4}$$

in which N_D is the donor concentration, and γ is a factor dependent on the material system and the device structure. And the piezo-gas sensing is much more effective than traditional modification of conductance (I−V behavior) as gas sensing at RT. The donor concentration of piezoelectric semiconductor will be changed by the surface adsorption of gas molecules, and the applied strain can be considered as signal amplification mechanism. Therefore, high sensitivity can be realized due to

DOI: 10.1021/acsami.5b01822
ACS Appl. Mater. Interfaces 2015, 7, 10482−10490

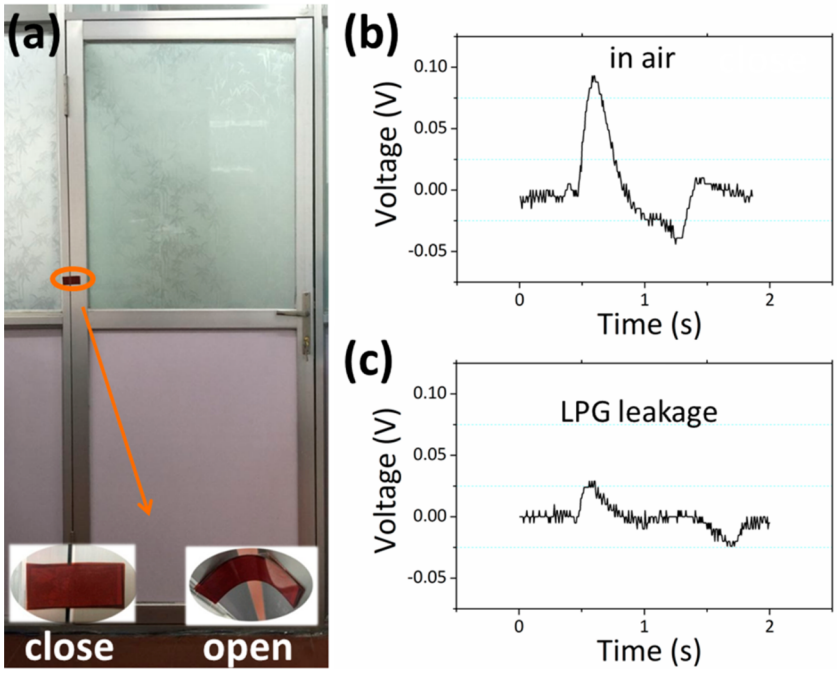

Figure 10. (a) $ZnSnO_3$/ZnO NW SPGS is stuck on a door, demonstrating its practical application. (b and c) Piezo-voltage of the SPGS (driven by opening the door) in air and LPG.

piezo-voltage acting as both power source and signal amplifier.[9,38]

Here, $ZnSnO_3$ nanoparticle layer can provide abundant of Lewis acid sites for gas adsorption and small value of activation energy for interaction.[20,39,40] Thus, the coupling effect between the surface effect of $ZnSnO_3$ and the piezo-screening effect of ZnO results in the RT-LPG sensing, as shown in Figure 9. Figure 9a and b show the piezo-surface coupling effect of $ZnSnO_3$/ZnO NWs in dry air. Without applied deformation (Figure 9a), $ZnSnO_3$/ZnO NWs have no strain and the SPGS has no piezoelectric output. The surface adsorption of oxygen molecules in air takes place on $ZnSnO_3$ nanoparticles through free electrons transporting from the nanoparticles to oxygen ions (O_2^-) as follows:[41−43]

$$O_2(\text{gas}) \leftrightarrow O_2(\text{adsorbed}) \quad (5,)$$

$$e^- + O_2(\text{adsorbed}) \leftrightarrow O_2^-(\text{chemisorbed}) \quad (6,)$$

As the compressive deformation is applied on the SPGS in air, $ZnSnO_3$/ZnO NWs have corresponding strain to generate piezoelectric field and the residual free electrons will have a piezo-screening effect on the output of the SPGS, as shown in Figure 9b. Figure 9c,d show the piezo-oxygen-sensing mechanism of $ZnSnO_3$/ZnO NW SPGS. In pure oxygen (Figure 9c), more oxygen molecules can be chemisorbed on $ZnSnO_3$ nanoparticle and capture more free electrons, significantly decreasing the electron density in the NWs. As the compressive deformation is applied on the SPGS in pure oxygen (Figure 9d), the fewer electrons in the NWs lead to a weaker piezo-screening effect on the piezoelectric output and result in a higher piezo-voltage than that in dry air. The piezo-LPG-sensing mechanism of $ZnSnO_3$/ZnO NW SPGS is shown in Figure 9e,f. LPG can decompose into reducing components with high reactivity on $ZnSnO_3$ surface because of the carbon-bound reducing hydrogen species in LPG molecules.[10] Thus, LPG molecules can be partially oxidized through the reaction with the chemisorbed O_2^- on $ZnSnO_3$ surface (forming gaseous species and water), as shown in Figure 9e.[17,39] The RT-LPG sensing of $ZnSnO_3$ nanoparticles is contributed by the abundant Lewis acid sites and the small value of activation energy (beneficial for both the surface adsorption of oxygen and the reaction between LPG and O_2^-). The overall reaction can be expressed as follows:[17,22,39,44]

$$C_nH_{2n+2} + O_2^-(\text{chemisorbed}) \rightarrow H_2O(\text{adsorbed}) + C_nH_{2n}\text{:O} + e^- \quad (7)$$

C_nH_{2n+2} includes C_4H_{10}, C_3H_8, and CH_4; and C_nH_{2n}:O is the partially oxidized intermediates.[22] This LPG-assisted removal of adsorbed oxygen and the generated water molecules displacement adsorption can increase the electron density in the NWs through releasing electrons back to the NWs from O_2^-. As the compressive deformation is applied on the SPGS in LPG (Figure 9f), the more electrons in the NWs lead to an enhanced piezo-screening effect, and result in a lower piezo-voltage than that in dry air.

LPG is explosive with a low concentration of 1.8% (18000 ppm), thus it is crucial for a person to realize the LPG leakage when opening the door. To simply demonstrate the practical application of $ZnSnO_3$/ZnO NW SPGS, a device (3 × 6 cm in area) is fixed on a door spindle (Figure 10a). The deformation on the device by opening the door is sufficient to generate piezoelectric output. For simulating the LPG leakage in the living environment, LPG is kept blowing to the device by an airbrush to ensure that the device is surrounded with LPG ambience. Figure 10b,c show the piezo-voltage of the SPGS driven by opening the door in air and LPG, respectively. In air and LPG, the piezo-voltage of the device is about 0.088 and 0.036 V, respectively, simply indicating the practical application of the SPGS. Future research efforts need to focus on designing new device structures with better practical applications, such as detecting the LPG leakage before opening a door.

DOI: 10.1021/acsami.5b01822
ACS Appl. Mater. Interfaces 2015, 7, 10482−10490

CONCLUSIONS

In summary, high sensitivity, selectivity, and reliability have been obtained from $ZnSnO_3$/ZnO NW SPGS for detecting LPG at RT. After being exposed to 8000 ppm LPG, the output piezo-voltage of $ZnSnO_3$/ZnO NWs under compressive deformation is 0.089 V, much smaller than that in air ambience (0.533 V). The sensitivity of the SPGS is up to 24.22, 31.16, 44.31, 67.52, 72.78, 79.72, 82.41, and 83.23 against 1000−8000 ppm LPG, respectively. The low limit of detection is 600 ppm. The SPGS can distinguish LPG from H_2S, H_2, ethanol, methanol, and saturated water vapor because the sensitivity against LPG is much higher than the others. During 2 months, the performance decline of the SPGS is merely 5.88%. Such RT-LPG sensing can be ascribed to the new piezo-surface coupling effect of $ZnSnO_3$/ZnO nanocomposites. The practical application of the device has also been simply demonstrated by mounting a device on a door. Our results point out a new way for realizing LPG sensing at RT.

AUTHOR INFORMATION

Corresponding Authors

* E-mail: yzhang@binn.cas.cn.
* E-mail: xuexinyu@mail.neu.edu.cn.

Notes

The authors declare no competing financial interest.

ACKNOWLEDGMENTS

This work was supported by the National Natural Science Foundation of China (51102041 and 11104025), the Fundamental Research Funds for the Central Universities (N120205001 and N140505004) and Program for New Century Excellent Talents in University (NCET-13-0112).

REFERENCES

(1) Dalton, R. Californian Labs Feel the Heat of Energy Crisis. *Nature* **2001**, *411*, 227−227.

(2) Tang, W.; Zhu, Y.; Hou, Y.; Liu, L.; Wu, Y.; Loh, K. P.; Zhang, H.; Zhu, K. Aqueous Rechargeable Lithium Batteries as an Energy Storage System of Superfast Charging. *Energy Environ. Sci.* **2013**, *6*, 2093−2104.

(3) Feng, S. H.; Xu, R. R. New Materials in Hydrothermal Synthesis. *Acc. Chem. Res.* **2001**, *34*, 239−247.

(4) Pope, C. A. Epidemiology of Fine Particulate Air Pollution and Human Health: Biologic Mechanisms and Who's at Risk? *Environ. Health Perspect.* **2000**, *108*, 713−723.

(5) Xu, S.; Qin, Y.; Xu, C.; Wei, Y.; Yang, R.; Wang, Z. L. Self-Powered Nanowire Devices. *Nat. Nanotechnol.* **2010**, *5*, 366−373.

(6) Ameen, S.; Akhtar, M. S.; Song, M.; Shin, H. S. Vertically Aligned ZnO Nanorods on Hot Filament Chemical Vapor Deposition Grown Graphene Oxide Thin Film Substrate: Solar Energy Conversion. *ACS Appl. Mater. Interfaces* **2012**, *4*, 4405−4412.

(7) Suematsu, K.; Shin, Y.; Hua, Z.; Yoshida, K.; Yuasa, M.; Kida, T.; Shimanoe, K. Nanoparticle Cluster Gas Sensor: Controlled Clustering of SnO_2 Nanoparticles for Highly Sensitive Toluene Detection. *ACS Appl. Mater. Interfaces* **2014**, *6*, 5319−5326.

(8) Wang, Y.; Du, G.; Liu, H.; Liu, D.; Qin, S.; Wang, N.; Hu, C.; Tao, X.; Jiao, J.; Wang, J.; Wang, Z. L. Nanostructured Sheets of Ti-O Nanobelts for Gas Sensing and Antibacterial Applications. *Adv. Funct. Mater.* **2008**, *18*, 1131−1137.

(9) Xue, X.; Nie, Y.; He, B.; Xing, L.; Zhang, Y.; Wang, Z. L. Surface Free-Carrier Screening Effect on the Output of a ZnO Nanowire Nanogenerator and Its Potential as a Self-Powered Active Gas Sensor. *Nanotechnology* **2013**, *24*, 225501.

(10) Gaikwad, N.; Bhanoth, S.; More, P. V.; Jain, G. H.; Khanna, P. K. Chemically Designed Pt/Ppy Nano-Composite for Effective LPG Gas Sensor. *Nanoscale* **2014**, *6*, 2746−2751.

(11) Maclean, H. L.; Lave, L. B. Evaluating Automobile Fuel/Propulsion System Technologies. *Prog. Energy Combust. Sci.* **2003**, *29*, 1−69.

(12) Chang, C. C.; Lo, J. G.; Wang, J. L. Assessment of Reducing Ozone Forming Potential for Vehicles Using Liquefied Petroleum Gas as an Alternative Fuel. *Atmos. Environ.* **2001**, *35*, 6201−6211.

(13) Qian, W. Z.; Yu, H.; Wei, F.; Zhang, Q. F.; Wang, Z. W. Synthesis of Carbon Nanotubes from Liquefied Petroleum Gas Containing Sulfur. *Carbon* **2002**, *40*, 2968−2970.

(14) Shinde, V. R.; Gujar, T. P.; Lokhande, C. D.; Mane, R. S.; Han, S.-H. Development of Morphological Dependent Chemically Deposited Nanocrystalline ZnO Films for Liquefied Petroleum Gas (LPG) Sensor. *Sens. Actuators, B* **2007**, *123*, 882−887.

(15) Gunjakar, J. L.; More, A. M.; Lokhande, C. D. Chemical Deposition of Nanocrystalline Nickel Oxide from Urea Containing Bath and Its Use in Liquefied Petroleum Gas Sensor. *Sens. Actuators, B* **2008**, *131*, 356−361.

(16) Salunkhe, R. R.; Dhawale, D. S.; Dubal, D. P.; Lokhande, C. D. Sprayed CdO Thin Films for Liquefied Petroleum Gas (LPG) Detection. *Sens. Actuators, B* **2009**, *140*, 86−91.

(17) Yadav, B. C.; Yadav, A.; Singh, S.; Singh, K. Nanocrystalline Zinc Titanate Synthesized via Physicochemical Route and Its Application as Liquefied Petroleum Gas Sensor. *Sens. Actuators, B* **2013**, *177*, 605−611.

(18) Ho Truong, G.; Ha Thai, D.; Pharn Quang, N.; Giang Hong, T.; Do Thi Anh, T.; Do Thi, T.; Nguyen Ngoc, T. Hydrocarbon Gas Sensing of Nano-Crystalline Perovskite Oxides $LnFeO_3$ (Ln = La, Nd and Sm). *Sens. Actuators, B* **2011**, *158*, 246−251.

(19) Barbero, B. P.; Gamboa, J. A.; Cadus, L. E. Synthesis and Characterisation of $La_{1-x}Ca_xFeO_3$ Perovskite-Type Oxide Catalysts for Total Oxidation of Volatile Organic Compounds. *Appl. Catal., B* **2006**, *65*, 21−30.

(20) Singh, S.; Singh, A.; Wan, M.; Yadav, R. R.; Tandon, P.; Rasool, S. S. A.; Yadav, B. C. Fabrication of Self-Assembled Hierarchical Flowerlike Zinc Stannate Thin Film and Its Application as Liquefied Petroleum Gas Sensor. *Sens. Actuators, B* **2014**, *205*, 102−110.

(21) Liu, Y. L.; Xing, Y.; Yang, H. F.; Liu, Z. M.; Yang, Y.; Shen, G. L.; Yu, R. Q. Ethanol Gas Sensing Properties of Nano-Crystalline Cadmium Stannate Thick Films Doped with Pt. *Anal. Chim. Acta* **2004**, *527*, 21−26.

(22) Singh, S.; Singh, A.; Yadav, B. C.; Dwivedi, P. K. Fabrication of Nanobeads Structured Perovskite Type Neodymium Iron Oxide Film: Its Structural, Optical, Electrical and LPG Sensing Investigations. *Sens. Actuators, B* **2013**, *177*, 730−739.

(23) Singh, R. C.; Singh, O.; Singh, M. P.; Chandi, P. S.; Thangaraj, R. Sensing Behaviour of Nanosized Zinc−Tin Composite Oxide toward Liquefied Petroleum Gas and Ethanol. *Mater. Res. Bull.* **2010**, *45*, 1162−1164.

(24) Sivapunniyam, A.; Wiromrat, N.; Myint, M. T. Z.; Dutta, J. High-Performance Liquefied Petroleum Gas Sensing Based on Nanostructures of Zinc Oxide and Zinc Stannate. *Sens. Actuators, B* **2011**, *157*, 232−239.

(25) Srivastava, A.; Rashmi; Jain, K. Study on ZnO-Doped Tin Oxide Thick Film Gas Sensors. *Mater. Chem. Phys.* **2007**, *105*, 385−390.

(26) Men, H.; Gao, P.; Zhou, B.; Chen, Y.; Zhu, C.; Xiao, G.; Wang, L.; Zhang, M. Fast Synthesis of Ultra-Thin $ZnSnO_3$ Nanorods with High Ethanol Sensing Properties. *Chem. Commun.* **2010**, *46*, 7581−7583.

(27) Zhang, Y.; Liu, Y.; Wang, Z. L. Fundamental Theory of Piezotronics. *Adv. Mater.* **2011**, *23*, 3004−3013.

(28) Sahay, P. P.; Nath, R. K. Al-Doped Zinc Oxide Thin Films for Liquid Petroleum Gas (LPG) Sensors. *Sens. Actuators, B* **2008**, *133*, 222−227.

(29) Chaudhari, G. N.; Bambole, D. R.; Bodade, A. B. Structural and Gas Sensing Behavior of Nanocrystalline $BaTiO_3$ Based Liquid Petroleum Gas Sensors. *Vacuum* **2006**, *81*, 251−256.

DOI: 10.1021/acsami.5b01822
ACS Appl. Mater. Interfaces 2015, 7, 10482−10490

(30) Gurav, K. V.; Patil, U. M.; Shin, S. W.; Pawar, S. M.; Kim, J. H.; Lokhande, C. D. Morphology Evolution of ZnO Thin Films from Aqueous Solutions and Their Application to Liquefied Petroleum Gas (LPG) Sensor. *J. Alloys Compd.* **2012**, *525*, 1−7.
(31) Roberts, S. Piezoelectric Effect in Lead Zirconate. *Phys. Rev.* **1951**, *83*, 1078−1078.
(32) He, J.; Lilley, C. M. Surface Effect on the Elastic Behavior of Static Bending Nanowires. *Nano Lett.* **2008**, *8*, 1798−1802.
(33) Lin, Y.; Deng, P.; Nie, Y.; Hu, Y.; Xing, L.; Zhang, Y.; Xue, X. Room-Temperature Self-Powered Ethanol Sensing of a Pd/ZnO Nanoarray Nanogenerator Driven by Human Finger Movement. *Nanoscale* **2014**, *6*, 4604−4610.
(34) Fu, Y.; Zang, W.; Wang, P.; Xing, L.; Xue, X.; Zhang, Y. Portable Room-Temperature Self-Powered/Active H_2 Sensor Driven by Human Motion through Piezoelectric Screening Effect. *Nano Energy* **2014**, *8*, 34−43.
(35) Hu, Y.; Zhang, Y.; Chang, Y.; Snyder, R. L.; Wang, Z. L. Optimizing the Power Output of a ZnO Photocell by Piezopotential. *ACS Nano* **2010**, *4*, 4220−4224.
(36) Liu, Y.; Yang, Q.; Zhang, Y.; Yang, Z.; Wang, Z. L. Nanowire Piezo-Phototronic Photodetector: Theory and Experimental Design. *Adv. Mater.* **2012**, *24*, 1410−1417.
(37) Gao, Y.; Wang, Z. L. Equilibrium Potential of Free Charge Carriers in a Bent Piezoelectric Semiconductive Nanowire. *Nano Lett.* **2009**, *9*, 1103−1110.
(38) Niu, S.; Hu, Y.; Wen, X.; Zhou, Y.; Zhang, F.; Lin, L.; Wang, S.; Wang, Z. L. Enhanced Performance of Flexible ZnO Nanowire Based Room-Temperature Oxygen Sensors by Piezotronic Effect. *Adv. Mater.* **2013**, *25*, 3701−3706.
(39) Singh, S.; Gupta, V.; Yadav, B. C.; Tandon, P.; Singh, A. K. Structural Analysis of Nanostructured Iron Antimonate by Experimental and Quantum Chemical Simulation and Its LPG Sensing. *Sens. Actuators, B* **2014**, *195*, 373−381.
(40) Koziej, D.; Bârsan, N.; Hoffmann, V.; Szuber, J.; Weimar, U. Complementary Phenomenological and Spectroscopic Studies of Propane Sensing with Tin Dioxide Based Sensors. *Sens. Actuators, B* **2005**, *108*, 75−83.
(41) Liu, Y.; Jiao, Y.; Zhang, Z.; Qu, F.; Umar, A.; Wu, X. Hierarchical SnO_2 Nanostructures Made of Intermingled Ultrathin Nanosheets for Environmental Remediation, Smart Gas Sensor, and Supercapacitor Applications. *ACS Appl. Mater. Interfaces* **2014**, *6*, 2174−2184.
(42) Hsu, C.-L.; Gao, Y.-D.; Chen, Y.-S.; Hsueh, T.-J. Vertical *p*-Type Cu-Doped ZnO/*n*-Type ZnO Homojunction Nanowire-Based Ultraviolet Photodetector by the Furnace System with Hotwire Assistance. *ACS Appl. Mater. Interfaces* **2014**, *6*, 4277−4285.
(43) Xing, L.-L.; Ma, C.-H.; Chen, Z.-H.; Chen, Y.-J.; Xue, X.-Y. High Gas Sensing Performance of One-Step-Synthesized Pd-ZnO Nanoflowers due to Surface Reactions and Modifications. *Nanotechnology* **2011**, *22*, 215501.
(44) Singh, S.; Yadav, B. C.; Gupta, V. D.; Dwivedi, P. K. Investigation on Effects of Surface Morphologies on Response of LPG Sensor based on Nanostructured Copper Ferrite System. *Mater. Res. Bull.* **2012**, *47*, 3538−3547.

DOI: 10.1021/acsami.5b01822
ACS Appl. Mater. Interfaces 2015, 7, 10482−10490